European Journal of Radiology Open 11 (2023) 100537

Contents lists available at ScienceDirect

European Journal of Radiology Open

journal homepage: www.elsevier.com/locate/ejro

Evaluation of three-dimensional dual-energy CT cholangiopancreatography image quality in patients with pancreatobiliary dilatation: Comparison with conventional single-energy CT

Bin Li, JianMing Ni, FangMing Chen, FengQi Lu, Lei Zhang, WenJuan Wu, ZhuiYang Zhang *

Department of Radiology, Wuxi No.2 People's Hospital, 68 Zhong shan Rd., Wuxi 214002, Jiangsu, PR China

HIGHLIGHTS

- This article is to describe a novel technique of multiphase fusion three-dimensional (3D) images in patients with malignant pancreatobiliary obstruction.
- Multiphase fusion 3D images of CT arteriography, portovenography and hepatic venography combined with negative-contrast CT cholangiopancreatography can be created with enhanced multiphase CT scan using intravenous contrast agent at one time.
- Preoperative one-stop evaluation of malignant pancreatobiliary obstruction may be feasible with this technique.

ARTICLE INFO

Keywords:
Negative-contrast CT
cholangiopancreatography
3D
Evaluation
Dual-energy CT
Iterative reconstruction
Single-energy CT
Pancreatobiliary dilatation

ABSTRACT

Objective: This study aimed to evaluate three-dimensional (3D) negative-contrast CT cholangiopancreatography (nCTCP) image quality using dual-energy CT (DECT) with iterative reconstruction (IR) technique in patients with pancreatobiliary dilatation compared with single-energy CT (SECT).

Methods: Of the patients, 67 and 56 underwent conventional SECT (SECT set) and DECT with IR technique (DECT set), respectively. All patients were retrospectively analyzed during the portal phase to compare objective image quality and other data including patient demographics, hepatic and pancreatic parenchymal enhancement, noise, and attenuation difference (AD) between dilated ducts and enhanced hepatic parenchyma, signal-to-noise ratio (SNR), contrast-to-noise ratio (CNR), and CT volume dose index ($CTDI_{vol}$). Two radiologists used the five-point Likert scale to evaluate the subjective image quality of 3D nCTCP regarding image noise, sharpness of dilated ducts, and overall image quality. Statistical analyses used the Mann–Whitney *U* test.

Results: No significant difference in patient demographics in either CT set was showed during objective evaluation ($p > 0.05$). However, higher hepatic and pancreatic parenchymal enhancement, AD, SNR, and CNR and lower hepatic and pancreatic noise ($p < 0.005$) as well as $CTDI_{vol}$ ($p = 0.005$) on DECT than on SECT were observed. Higher mean grades on DECT than on SECT were showed for image noise (4.65 vs 3.92), sharpness of dilated ducts (4.52 vs 3.94), and overall image quality (4.45 vs 3.91; $p < 0.001$), respectively during subjective evaluation.

Conclusion: A higher overall image quality and lower radiation dose on 3D nCTCP can be obtained by DECT with IR technique than with conventional SECT in patients with pancreatobiliary dilatation.

1. Introduction

Pancreatobiliary dilatation can be secondary to either benign or malignant processes. Further determination of the causes of a dilated pancreatobiliary system is very important in managing this condition [1]. As a well-established noninvasive technique for assessing the biliary tract, magnetic resonance cholangiopancreatography (MRCP) has been widely used in daily practice because of its high sensitivity and specificity for diagnosing suspected obstructive biliary diseases or strictures given the presence of pancreatobiliary dilatation [2–5]. However, additional sequences are required with contrast-enhanced imaging when assessing noncalculous obstruction [3,6–8]. The main limitations

* Correspondence to: Department of Radiology, Wuxi No.2 People's Hospital, 68 Zhongshan Rd., Jiangsu 214002, PR China.
E-mail address: zhangzhuiyang@163.com (Z. Zhang).

https://doi.org/10.1016/j.ejro.2023.100537
Received 14 July 2023; Received in revised form 18 October 2023; Accepted 24 October 2023

of MRCP are unable to evaluate extraductal structures and have relatively lower spatial resolution on two-dimensional (2D), or motion artifacts on breath-hold three-dimensional (3D) MRCP in patients with irregular breathing patterns [3,9]. Furthermore, some contraindications (e.g., pacemarker, aneurysm clips, or claustrophobia) on MR imaging limit its use [4,6]. Meanwhile, computed tomography (CT) commonly represents a first- or second-line diagnostic tool in patients with abdominal disorders involving the bile duct system [6,10]. In addition, appropriate dilatation of the pancreatobiliary ducts during the portal phase can be used to extract pixels for 3D negative-contrast CT cholangiopancreatography (nCTCP) with minimum intensity projection (MinIP) to depict the pancreatobiliary system similar to MRCP [4,7,8]. It allows to correctly determining the level and cause of biliary obstruction as well as an improvement of visualization of the pancreaticobiliary system [4,8,11]. With the advent of multidetector-row CT (MDCT, especially $\geq$ 64 MDCT), high-quality 2D reformatted images along with nCTCP can be acquired simultaneously when submillimeter volume data are obtained [7,8,12–14].

Nevertheless, the 3D nCTCP image quality largely depends on the attenuation difference (AD) between dilated ducts and enhanced hepatic and pancreatic parenchyma. Therefore, maximal hepatic and pancreatic parenchymal enhancement is one of the most important factors [6,11]. Several approaches (e.g., increasing iodine concentration or dose and injection flow) were previously attempted to improve hepatic and pancreatic parenchymal enhancement. The main limitations of these methods are the greater renal impact and the simultaneous risk of contrast agent extravasation [15,16]. Recently, dual-energy CT (DECT) with iterative reconstruction (IR) has been applied in clinical practice. A weighted-average image that simulates the image quality of a standard 120-kVp acquisition can be reconstructed from the two datasets with low- and high-energy acquisition techniques. This blended image ensures acceptable image quality and preserves low-contrast detectability, which improves the contrast-to-noise ratio (CNR) and aids in detecting and characterizing lesions [17,18]. Moreover, IR can enable the use of reduced-dose CT, decrease noise and increase contrast in CT images [19–21].

Thus, the hypothesis of this study was that DECT with the IR technique may improve 3D nCTCP image quality while reducing the radiation dose, which will be helpful in providing more accurate information concerning the pancreaticobiliary ducts in clinical practice. Given this, the purpose of the study is to evaluate 3D nCTCP image quality using DECT with IR in patients with pancreatobiliary dilatation compared with conventional single-energy CT (SECT).

2. Materials and methods

2.1. Patients

This retrospective study was performed in compliance with the guidelines of the Health Insurance Portability and Accountability Act and approved by the institutional review board of this study. Written informed consent was obtained from all patients. From January 2016 to February 2020, data regarding 453 consecutive patients with clinical findings of abdominal pain, jaundice, weight loss, or abnormal laboratory results (e.g., elevated total serum bilirubin and/or alkaline phosphate levels) were collected from the image archive and communication system. Among these patients, 294 and 159 patients underwent conventional SECT (Aquilion 64, Toshiba Medical Systems) and DECT during the portal phase (Aquilion ONE, Toshiba Medical Systems) of the abdomen, respectively. The inclusion criteria for pancreatobiliary dilatation were adopted from a previous report: the common bile duct or common hepatic duct diameter $>$ 6 mm if the gallbladder was present and the patient was $<$ 60 years old with or without intrahepatic ductal dilatation. If the patient was $\geq$ 60 years old, 1 mm was added to the upper limit for every additional decade of life over 60 years. If the gallbladder was absent, biliary ductal dilatation was defined as an extrahepatic bile duct diameter $>$ 10 mm for all ages [1]. The exclusion criteria included nondilated ducts, substantial motion artifacts that produced images that were nondiagnostic quality, failure in CT enhancement (e.g., because of contrast agent extravasation), and section thickness $\geq$ 1.0 mm. In this study, the standard section thickness for abdominal scan was 1.0 mm with Aquilion 64 (64-MDCT), and 0.5 mm with Aquilion ONE (320-MDCT). However, 0.5 mm section thickness was used in patients with suspected pancreatobiliary diseases because preferably submillimeter is recommended for high-fidelity reformatted and volumetric images from near isotropic voxel acquisition [12–14]. Thus, 227 and 103 patients from the conventional SECT (SECT set) and DECT (DECT set), respectively, were excluded. Consequently, 67 (34 males and 33 females; mean age, 66.7 years; range, 31–89 years) and 56 (29 males, 27 females; mean age, 65.0 years; range, 41–93 years) patients in the SECT and DECT sets were enrolled in this study, respectively. The flow chart for patient selection is illustrated in Fig. 1, and the benign-malignant causes of pancreaticobiliary dilatation confirmed by endoscopy or pathology in the two CT sets are listed in Table 1.

2.2. CT examinations

In both SECT and DECT sets, nonenhanced and dual-phase enhanced CT were performed in all patients. Moreover, 500–800 mL water was orally administered 30 min before CT examinations. All patients were administered a nonionic contrast agent (1.5 mL/kg, and maximum volume of 100 mL ioversol; Optiray 320, Tyco Health care) via a power injector at a flow of 4 mL/s for dual-phase enhanced CT. An automatic trigger scanning mode with a 10- to 15-s delay was used to acquire the late arterial phase when a region of interest (ROI) was set on the descending aorta in which the preset CT number was 200 in Hounsfield units (HU). In this mode, the late arterial and portal phases were delayed by 35–45 s and 65–75 s, respectively, after the initiation of contrast administration. Specifically, only the portal phase acquisition used sequential dual-energy (80/135 kVp) in the helical scan mode in the DECT set. In this study, the image quality analysis of 3D nCTCP was based on portal phase data [22]. The detailed scan parameters for the two CT sets are listed in Table 2.

2.3. Image processing and analysis

In the SECT dataset, the portal phase raw data were reconstructed with both a section thickness and an interval of 0.5 mm with the standard filtered back projection (FBP) and a kernel of FC 02. In contrast, the DECT set raw data were reconstructed using the same section thickness and interval as used in the SECT set with the IR technique of an adaptive iterative dose reduction system using a 3D processing algorithm (AIDR 3D) and a kernel of FC 17. Although energy-specific postprocessing methods, such as optimized monoenergetic (e.g., 60–70 keV) methods, can lead to better image quality than a conventional 120-kVp technique with the same radiation dose, this improvement may not be confirmed until the images obtained using this approach are compared with SECT acquisitions using lower-tube voltage settings (e.g., 80 kVp) [17]. Therefore, this study used nonmaterial-specific image (also referred to as blended images) reconstruction with a nonlinear blending mode, which combines the data from the low- and high-energy images in a single dataset as a weighted-average image equivalent to a conventional single-energy 120-kVp acquisition and takes advantage of both the high-contrast contribution from the lower-energy dataset (80 kVp) and the low noise levels from the high-energy dataset (135 kVp). Thus, quantum noise and iodine contrast CNR are minimized and maximized, respectively [17].

All reconstructed 2D source images (volume data) during the portal phase were then transferred to a dedicated workstation (Advantage Workstation, version 4.6, GE Healthcare). A trained radiologist (with 10 years of experience in abdominal CT) undertook the CT image postprocessing at the workstation. 3D nCTCP images were generated with

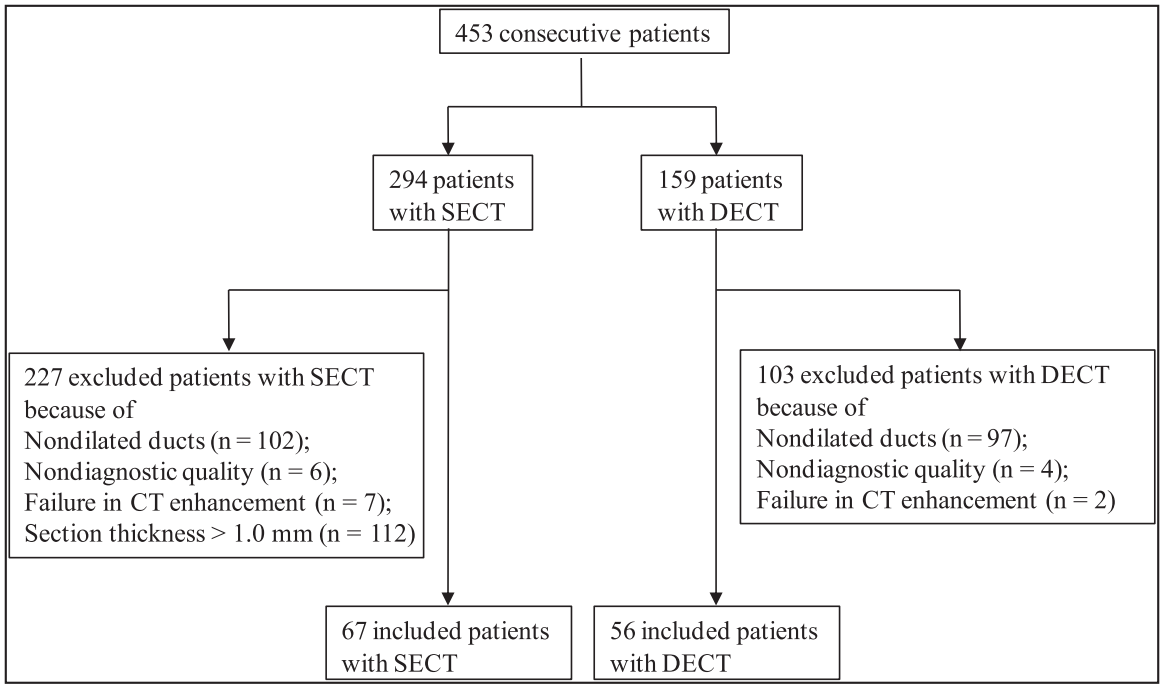

Fig. 1. Flow chart for patient selection.

Table 1
Causes of pancreaticobiliary dilatation in the two CT sets.[a].

SECT set (n = 67)	DECT set (n = 56)
Benign (n = 27)	Benign (n = 24)
CBD stone (n = 19)	CBD stone (n = 12)
BAS (n = 4)	BAS (n = 8)
Duodenal diverticulum (n = 2)	AIP (n = 1)
Acute pancreatitis (n = 1)	Mucinous cystadenoma (n = 2)
Pancreatic pseudocyst (n = 1)	Choledochal cyst (n = 1)
Malignant (n = 40)	Malignant (n = 32)
HCCC (n = 9)	HCC (n = 1)
Gallbladder carcinoma (n = 2)	ICC (n = 1)
DBDC (n = 5)	HCCC (n = 4)
PHC (n = 10)	Gallbladder carcinoma (n = 1)
Ampullary carcinoma (n = 10)	DBDC (n = 5)
Duodenal carcinoma (n = 3)	PHC (n = 13)
Metastasis (n = 1)	Ampullary carcinoma (n = 6)
	Duodenal carcinoma (n = 1)

CBD, common bile duct; BAS, benign ampullary stenosis; HCC, hepatocellular carcinoma; ICC, intrahepatic cholangiocarcinoma; HCCC, hilar cholangiocarcinoma; DBDC, distal bile ductal carcinoma; PHC, pancreatic head carcinoma; AIP, autoimmune pancreatitis.

[a] For comparisons for benign-malignant causes of pancreaticobiliary dilatation in the two CT sets were used the Chi-square test ($p = 0.855$)

Table 2
Scan and reconstruction parameters in the two CT sets.

Parameter	SECT set	DECT set
Scan		
Detector configuration	64 × 0.5 mm	80 × 0.5 mm
kVp	120	135/80
mA	automatic tube current	100/570
Tube rotation	0.5 s	0.35 s
Pitch	27	9.4
FOV	30–40 cm^2	30–40 cm^2
Reconstruction		
Section thickness	0.5 mm	0.5 mm
Section internal	0.5 mm	0.5 mm
FOV	24–33 cm^2	25–35 cm^2
Matrix	512 × 512	512 × 512
Kernel	FC 02	FC 17
Algorithm	FBP	AIDR 3D

FBP, filtered back projection; FOV, field of vision; AIDR 3D, adaptive iterative dose reduction using 3D processing.

3D tools as previously described [7]. However, this study used the segment tool in the *Paint on slices* for analysis, which can be used to independently segment multiple regions, such as the liver, pancreas, and duodenum, from other abdominal lower attenuations (fat, air, etc.) on the same edited image. The adjustment of the edited slab thickness each time can be controlled by the mouse scroll wheel based on the dilated pancreatobiliary system. The extra time for 3D nCTCP in this study was 10–15 min (mean, 12 min) with a total segmented width of 90 mm (range, 70–150 mm).

2.4. Objective image quality evaluation

All patient demographics, including sex ratio, body weight, age, height, body mass index (BMI) [BMI = weight (kg)/height (m^2)], and volume CT dose index ($CTDI_{vol}$, mGy) as well as CT numbers obtained in the liver, pancreas, dilated extrahepatic or intrahepatic bile ducts, perirenal fat (as background) in the axial image, and their image noise defined as the standard deviation (SD) during the portal phase were recorded by the radiologist during analyses of the two CT sets. For the same patient, an ROI of approximately 20 mm was placed in the liver, pancreas, dilated extrahepatic or intrahepatic bile ducts, and perirenal fat. Moreover, a smaller size was used when 20 mm ROI placement was not possible [22]. To prevent measurement errors, the ROI cursors were kept away from intrahepatic or pancreatic hyper (e.g., vasculature or calcification) or hypo-(e.g., fat or dilated ducts) attenuated structures. Otherwise, all measurements were performed twice, and mean values were calculated. The signal-to-noise ratio (SNR) and CNR for the hepatic and pancreatic parenchyma were calculated using the following formulas: $SNR_{liver,\ pancreas} = ROI_{liver,\ pancreas}/SD_{liver,\ pancreas}$ and $CNR_{liver,\ pancreas} = ROI_{liver,\ pancreas} - ROI_{background}/SD_{background}$.The ROI denotes the attenuation values (HU) of the liver or pancreas. The SD and ROI background denotes the image noise and attenuation of fat, respectively [22]. Furthermore, AD = CT $attenuation_{liver}$ (HU)− CT $attenuation_{bile\ ducts}$ (HU) was used to compare the AD between dilated bile ducts and

enhanced hepatic parenchyma in the two CT sets.

2.5. Subjective image quality evaluation

Two other radiologists (with 10 and 13 years of experience in abdominal CT) blinded to the acquisition parameters used to analyze the two CT sets independently evaluated the 3D nCTCP image quality on the same workstation in a randomized order. A five-point Likert scale was used to rate the image noise (1, unacceptable; 2, above average; 3, average; 4, less than average; and 5, minimal), sharpness of dilated ducts, and overall image quality (1, unacceptable; 2, fair; 3, moderate; 4, good; and 5, excellent) [23]. For example, a grade 1 in the overall image quality may represent a nondiagnostic image with unacceptable noise, poor SNR, CNR, or interfering elements overlap from the surrounding structures (e.g., fat or air) [6] wherein the dilated ductal system is hardly distinguishable; grade 3 (moderate) represents an acceptable image with diagnostic image quality; and grade 5 (excellent image quality) indicates an image with the best SNR and CNR and in which any interfering elements overlapping on the image is scarce. After the first independent image analysis, interobserver agreement was assessed for each CT imaging finding. In this study, the agreement for both observers served as the final evaluation result. For discordant imaging evaluations, another radiologist (with 18 years of experience in abdominal CT) combined the two CT sets and decided which results to use after reviewing the images [24].

2.6. Statistical analysis

Statistical analyses in the two CT sets were performed using MedCalc Software for Microsoft Windows (version 9.6.2.0). For benign-malignant causes of pancreaticobiliary dilatation were compared using the Chi-square test. Both objective and subjective variables are expressed as the mean ± SD except for the sex ratio. Considering that the variances originated from two independent samples, the Mann–Whitney *U* test was used to evaluate the significance of the objective and subjective variables [25]. Results with a p value < 0.05 were considered statistically significant. Weighted kappa analysis was performed to assess interobserver agreement for subjective evaluation of the image quality. Kappa values < 0.20, 0.20–0.39, 0.40–0.59, 0.60–0.79, and ≥ 0.80 indicated poor, fair, moderate, good, and excellent agreement, respectively [8].

3. Results

3.1. General comparison

There was no statistical difference between benign-malignant causes of pancreaticobiliary dilatation in the two CT sets ($p = 0.855$) (Table 1). The outcomes of the comparison of the two CT sets for patient demographics and objective evaluation are summarized in Table 3. Differences in the demographic information, including the patient's sex ratio, age, height, weight, and BMI, were all statistically insignificant ($p > 0.05$) in both CT sets. However, $CTDI_{vol}$ differed significantly ($p = 0.005$), and the DECT set showed a lower radiation dose than the SECT set.

3.2. Objective data comparison

In the objective image quality evaluation, the hepatic and pancreatic CT numbers, AD, SNR, and CNR were significantly higher in the DECT set than in the SECT set ($p < 0.001$) (Fig. 2). In addition, both the hepatic and pancreatic parenchymal noise were also significantly lower ($p < 0.005$) in the DECT set than in the SECT set.

Table 3
Comparison of patient demographics and radiation dose as well as objective evaluation between the two CT sets.

Variable	SECT set	DECT set	*p*-value
Sex			0.921
Male	34	29	
Female	33	27	
Age (years)	67.66 ± 12.15	65.02 ± 10.59	0.106
Height (m)	1.62 ± 0.08	1.63 ± 0.08	0.532
Weight (kg)	58.25 ± 11.10	59.21 ± 9.96	0.382
BMI (kg/m^2)	22.10 ± 3.50	22.17 ± 2.99	0.709
$CTDI_{vol}$ (mGy)	21.60 ± 5.24	20.79 ± 1.63	0.005
CT $attenuation_{liver}$(HU)	100.42 ± 15.46	138.54 ± 20.95	< 0.001
$Noise_{liver}$(HU)	19.59 ± 3.67	17.92 ± 4.25	0.003
CT $attenuation_{pancreas}$(HU)	96.04 ± 17.15	132.29 ± 21.38	< 0.001
$Noise_{pancreas}$(HU)	20.48 ± 3.83	17.49 ± 4.26	< 0.001
$AD_{liver–bile\ ducts}$(HU)	95.90 ± 14.97	122.59 ± 20.20	< 0.001
SNR_{liver}	5.34 ± 1.36	8.11 ± 2.11	< 0.001
CNR_{liver}	11.05 ± 3.23	14.31 ± 3.55	0.001
$SNR_{pancreas}$	4.090 ± 1.44	7.98 ± 1.93	< 0.001
$CNR_{pancreas}$	10.83 ± 723	13.95 ± 3.43	< 0.001

Data are the mean ± standard deviation (SD) except for the sex ratio. BMI, body mass index; CTDIvol, volume CT dose index; HU, Hounsfield units; AD, attenuation difference; SNR, signal-to-noise ratio; CNR, contrast-to-noise ratio.

3.3. Subjective data comparison

In the subjective image quality evaluation, the DECT set showed higher mean grades than the SECT set for image noise (4.65 vs 3.92), sharpness of dilated ducts (4.52 vs 3.94), and overall image quality (4.45 vs 3.91) (Figs. 3, 4), and significant differences were noted in both CT sets ($p < 0.001$) (Table 4). In the SECT set, the overall image quality was graded as excellent, good, and moderate in 5/67 (7.5%), 51/67 (76.1%), and 11/67 (16.4%) patients, respectively, unlike the proportions of 29/56 (51.8%), 24/56 (42.9%), and 3/56 (5.3%) patients in the DECT set. Eleven patients with moderate overall image quality had images with higher image noise (eight patients) or more fat elements from pancreatic fatty infiltration (three patients) overlapping on images in the SECT set. However, higher image noise was observed in one patient, and the other two had images exhibiting fat elements overlapping on the image in the DECT set.

3.4. Interobserver agreement

Interobserver agreement for subjective evaluation of image noise, sharpness of dilated ducts, and overall image quality in the DECT set was excellent, with kappa values of 0.806, 0.800, and 0.817, respectively. Correspondingly, interobserver agreement was good to excellent in analyses of the SECT set, with kappa values of 0.756, 0.693, and 0.812.

4. Discussion

Over the past decade, published studies regarding nCTCP have been performed either in conventional single-slice CT or MDCT with the standard FBP reconstruction algorithm [2–4,6–8,11,26]. The ability to improve the identification of obstructive or stricture sites and causes, assist in the classification of malignant perihilar obstruction, and depict complex biliary anatomy or variants in patients with obstructive diseases has been demonstrated [7,8,26]. Thus, this approach represents a valuable supplement to conventional CT images and makes MDCT a one-step evaluation of hepatopancreatic disorders [2,3,6].

Advances in CT technology have enabled the application of DECT in clinical practice, including rapid kilovoltage peak switching, multilayer detectors, and sequential helical mode. Unlike conventional SECT, DECT can be used to concurrently acquire MDCT data at low and high energies in a single acquisition. Moreover, the results of the diagnostic evaluation of images from DECT datasets can be displayed using nonmaterial specific, material specific, and energy-specific display methods [17]. For

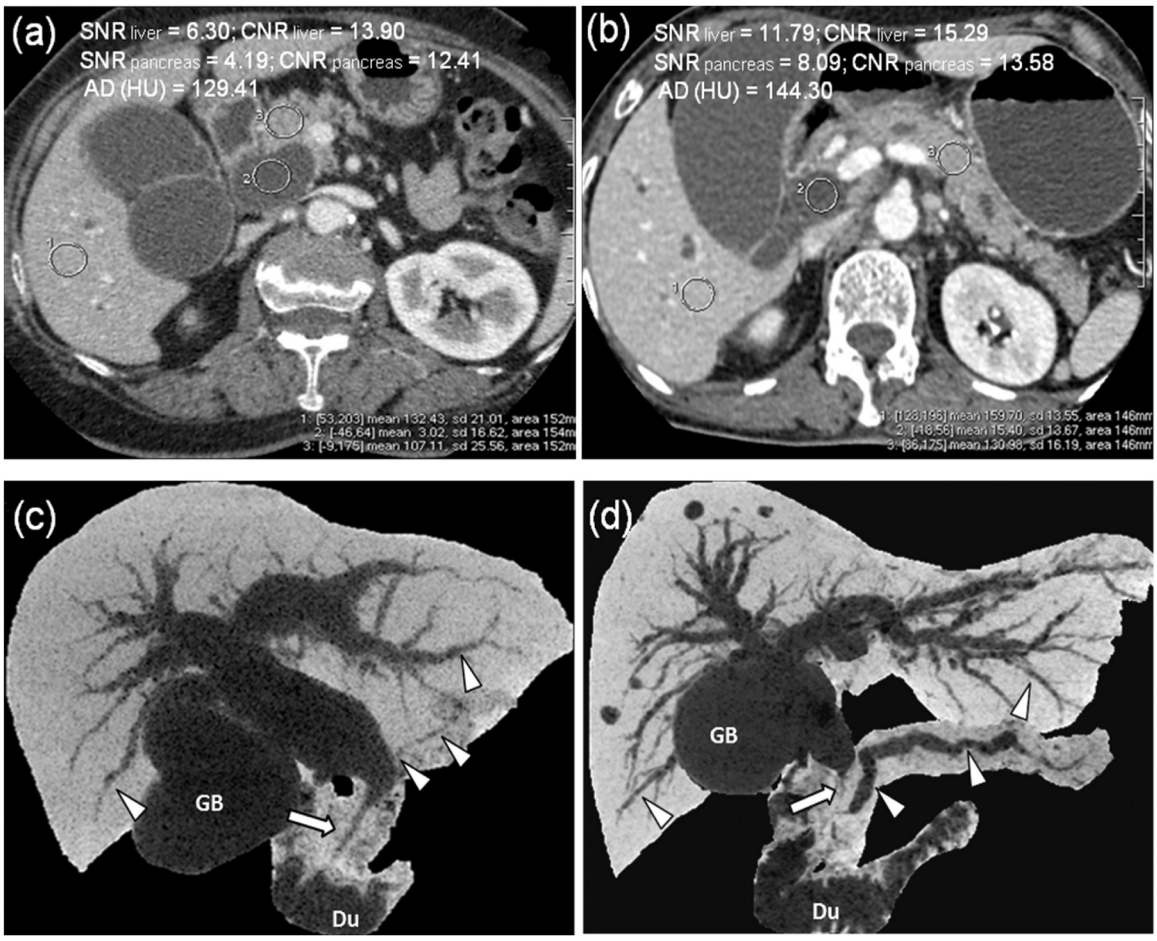

Fig. 2. Dilated ducts secondary to distal bile duct carcinomas confirmed by pathology. An objective image quality evaluation of a SECT image (A) in a 68-year-old female with a BMI of 20.39 and DECT image (B) in a 72-year-old female with a BMI of 20.96 on axial images during the portal phase shows that the hepatic and pancreatic parenchyma has a higher CT number and AD but lower noise on DECT than on SECT. Both the SNR and CNR on DECT were also higher than those on SECT in the two patients. Subjective evaluation of 3D nCTCP with MinIP image quality from SECT (C) and DECT (D) shows abrupt strictures of the distal common bile duct on both 3D nCTCPs (arrows), however, an almost imperceptible image noise, sharper intrahepatic and pancreatic ductal margins (arrowheads), and better overall image quality on DECT vs SECT (all grades of 5 vs 4). Du, duodenum; GB, gallbladder.

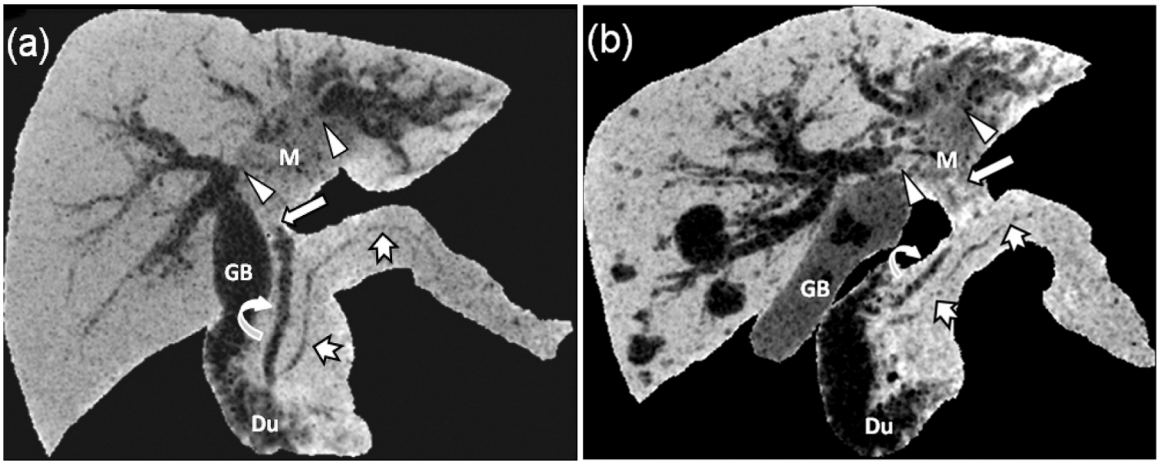

Fig. 3. Intrahepatic ductal dilatation secondary to hilar cholangiocarcinomas confirmed by pathology. 3D nCTCP with MinIP images from SECT (A) in a 68-year-old female with a BMI of 20.54 and DECT (B) in a 65-year-old male with a BMI of 22.10. Comparisons of subjective image quality between DECT and SECT images demonstrate a slightly lower background noise (grade of 5 vs 4), sharper intrahepatic ductal margin (grade of 5 vs 4), and overall image quality (grade of 5 vs 4). Both CT sets depict that mass (M) involved the secondary confluence of both the right (arrowheads) and left hepatic ducts as well as common hepatic ducts (arrows). The nondilated common bile ducts (curved arrows) and duct segments of the pancreatic head and body (tailed arrows) are also shown. Du, duodenum; GB, gallbladder.

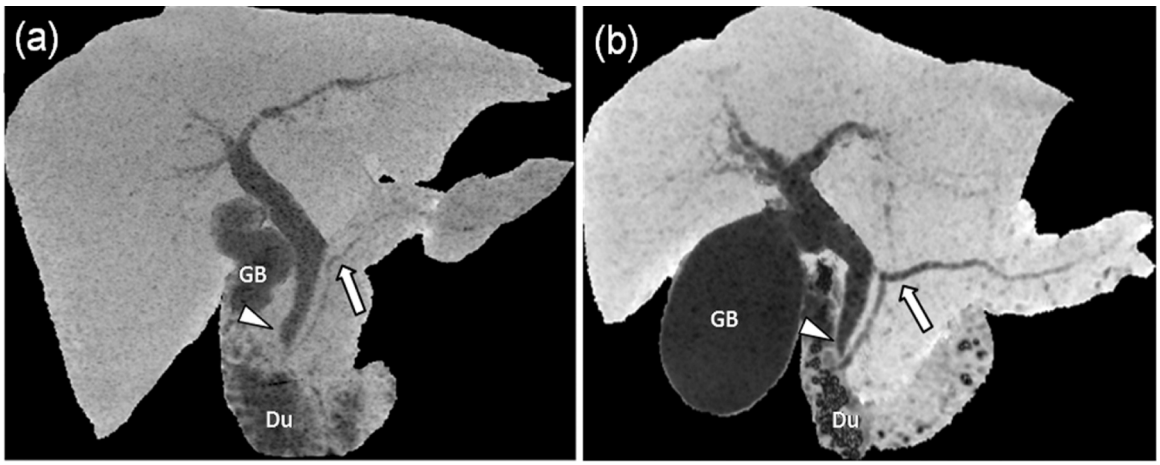

Fig. 4. Slightly biliary dilatation secondary to benign ampullary stenoses confirmed by endoscopy. 3D nCTCP with MinIP images from SECT (A)in a 67-year-old female with a BMI of 17.48 and DECT (B)in an85-year-old female with a BMI of 18.03. Subjective image quality evaluation on DECT demonstrates lower image noise (grade of 5 vs 4), sharper extrahepatic bile duct (arrowheads) and pancreatic duct (arrows) (grade of 5 vs 4) as well as better overall image quality than on SECT (grade of 5 vs 4). Both CT sets show a typically benign sign—gradual tapering of the common bile duct (arrowheads). Du, duodenum; GB, gallbladder.

Table 4
Comparison of subjective image quality evaluation results between the two CT sets.

Variable	SECT set	DECT set	*p*-value
Image noise	3.92 ± 0.47	4.65 ± 0.52	< 0.001
Sharpness of dilated ducts	3.94 ± 0.52	4.52 ± 0.57	< 0.001
Overall image quality	3.91 ± 0.49	4.45 ± 0.60	< 0.001

routine diagnostic interpretation, blended images can be reconstructed based on nonmaterial-specific images, which combine the data from the low- and high-energy images in a single dataset and take advantage of both high CNR from the lower-energy dataset and the low noise levels from the high-energy dataset [17,18]. In this study, we used sequential DECT in helical scan mode, and the acquired DECT datasets were reconstructed with a nonlinear blending technique, which works in the image-space domain to maximize the contribution from the high-contrast low-energy dataset. Thus, this technique leads to better subjective perception of image quality by the reader than a conventional linear blending technique in DECT [17].

In the subjective image quality evaluation, the initial results of this study demonstrated that the DECT set showed significantly higher hepatic and pancreatic parenchymal enhancement, AD, SNR, and CNR than the SECT set. Lower hepatic and pancreatic parenchymal noise in the DECT set than in the SECT set was also observed.

In the subjective image quality evaluation, the DECT set showed lower image noise, sharper pancreatobiliary duct margins, and higher overall image quality than the SECT set (all $p < 0.001$). Although higher image noise may be associated with a higher BMI since patients evaluated as having moderate overall image quality possessed a BMI greater than the mean BMI in both CT sets, only one of three patients who were evaluated as having images of moderate overall image quality in the DECT set presented image quality affected by image noise, unlike eight of 11 patients in the SECT set. Accordingly, DECT could be used to substantially aid in increasing AD between the bile ducts, enhancing hepatic and pancreatic parenchyma, and further leading to better 3D nCTCP image quality than conventional SECT in the present study.

The radiation dose from DECT must be considered when comparing the radiation dose from conventional SECT acquisition [19,20]. This study used DECT with the AIDR 3D technique. Although the two CT sets with mean $CTDI_{vol}$ were all below the American College of Radiology's 25-mGy reference level for a single-phase abdominal CT [27], a significantly lower mean $CTDI_{vol}$ was noted in the DECT set than in the SECT set with an FBP reconstruction technique ($p = 0.005$). The SNR is improved while the spatial resolution is preserved, and natural-looking images are produced because AIDR 3D can incorporate unique noise reduction processing, which include statistical and scanner models for projection data and multiple cycles of information syntheses with edge-handling, smoothing, and blending of original input images until the final output images are created [28,29].

Considering the strengths of both DECT with improving in CNR and IR with increasing in SNR and decreasing in noise [17,18,21], higher overall image quality on 3D nCTCP may attribute to a synthesis of DECT and IR in this study. It is true that further determination of the causes of the dilated pancreatobiliary system was not performed in this study because this study aimed to evaluate the image quality achieved using 3D nCTCP using DECT acquisition with the IR technique and to compare this approach with conventional SECT. However, we speculate that the better 3D nCTCP image quality may have the potential for improving the identification of the causes of dilated pancreatobiliary systems, such as locating iso-attenuation pancreatic mass, differentiating ampullary carcinoma from pancreatic head carcinoma or benign-malignant causes on the basis of the dilated pancreatic duct in patients with pancreatic pathologies when combined with 2D images [7,8,30].

Several limitations in the present study should be addressed. First, the manual edition of 3D nCTCP is still a time-consuming procedure, unlike thin-slab MinIP or MPR imaging [6]. However, this limitation may be gradually controlled in the future with automatic multiorgan segmentation techniques [31,32]. Furthermore, the sequential DECT helical scan mode was used in this study. However, the delay time between acquisitions results in misregistration of respiratory motions and temporal variation in contrast opacification [18]. Consequently, a longer scan time may not be favorable for dose reduction [33]. This problem will be resolved with the newest-generation DECT scanner and IR [34]; finally, monoenergetic (e.g., 60–70 keV) image quality with SECT was not compared. Therefore, further comparative studies with monoenergetic data for 3D nCTCP on DECT may be needed, although this approach is still controversial [17].

In conclusion, the initial results of this study demonstrated that higher overall 3D nCTCP image quality and lower radiation dose can be obtained by using dual-energy acquisition with the AIDR 3D technique than by using conventional single-energy acquisition.

Funding statement

This study was funded by "Wuxi Taihu Lake Talent Plan, Leading

Talents in Medical and Health Profession (2020)".

Ethical statement

This study meets the requirements of the Declaration of Helsinki.

CRediT authorship contribution statement

Ni JianMing: Supervision, Conceptualization. **Chen FangMing:** Data curation. **Li Bin:** Writing – original draft, Methodology, Investigation. **Wu WenJuan:** Formal analysis, Data curation. **Zhang ZhuiYang:** Writing – review & editing, Funding acquisition, Conceptualization. **Lu FengQi:** Resources, Project administration. **Zhang Lei:** Resources, Methodology.

Declaration of Competing Interest

The authors declare that they have not an actual or potential conflict of interest including any financial, personal or other relationships with other people or organization, that can inappropriately influence the work.

References

[1] J.S. Chalfan, A.W. Skaggs, T.W. Loehfelm, G. Fananapazir, M.T. Corwin, Incidentally detected biliary ductal dilatation on contrast-enhanced CT: what is the incidence of occult obstructing malignancy? Abdom. Radiol. 44 (12) (2019) 4022–4027, https://doi.org/10.1007/s00261-019-02217-7.

[2] F. Zandrino, L. Benzi, M.L. Ferretti, R. Ferrando, G. Reggiani, F. Musante, Multislice CT cholangiography without biliary contrast agent: technique and initial clinical result in the assessment of patients with biliary obstruction, Eur. Radiol. 12 (5) (2002) 1155–1161, https://doi.org/10.1007/s00330-001-1188-y.

[3] F. Zandrino, P. Curone, L. Benzi, M.L. Ferretti, F. Musante, MR versus multislice CT cholangiography in evaluating patients with obstruction of the biliary tract, Abdom. Imaging 30 (1) (2005) 77–85, https://doi.org/10.1007/s00261-004-0227-y.

[4] Z.Y. Zhang, D. Wang, J.M. Ni, X.R. Yu, L. Zhang, W.J. Wu, L. Gong, M.H. Hu, Comparison of three-dimensional negative-contrast CT cholangiopancreatography with three-dimensional MR cholangiopancreatography for the diagnosis of obstructive biliary diseases, Eur. J. Radiol. 81 (5) (2012) 830–837, https://doi.org/10.1016/j.ejrad.2011.02.036.

[5] B.S. Kapoor, G. Mauri, J.M. Lorenz, Management of biliary strictures: state-of-the-art review, Radiology 289 (3) (2018) 590–603, https://doi.org/10.1148/radiol.2018172424.

[6] T. Denecke, E. Degutyte, L. Stelter, L. Lehmkuhl, R. Valencia, L.E. opez-Hänninen, R. Felix, C. Stroszczynski, Minimum intensity projections of the biliary system using 16-channel multidetector computed tomography in patients with biliary obstruction: comparison with MRCP, Eur. Radiol. 16 (8) (2006) 1719–1726, https://doi.org/10.1007/s00330-006-0172-y.

[7] B. Li, L. Zhang, Z.Y. Zhang, J.M. Ni, F.Q. Lu, W.J. Wu, C.J. Jiang, Differentiation of noncalculous periampullary obstruction: comparison of CT with negative-contrast CT cholangiopancreatography versus MRI with MR cholangiopancreatography, Eur. Radiol. 25 (2) (2015) 391–401, https://doi.org/10.1007/s00330-014-3430-4.

[8] F.M. Chen, J.M. Ni, Z.Y. Zhang, L. Zhang, B. Li, C.J. Jiang, Presurgical evaluation of pancreatic cancer: a comprehensive imaging comparison of CT versus MRI, AJR Am. J. Roentgenol. 206 (3) (2016) 526–535, https://doi.org/10.2214/AJR.15.15236.

[9] Z.Y. Chen, B. Sun, Y.J. Xue, Q. Duan, E.S. Zheng, Y.Y. He, G.J. Li, Z.S. Zhang, Comparing compressed sensing breath-hold 3D MR cholangiopancreatography with two parallel imaging MRCP strategies in main pancreatic duct and common bile duct, Eur. J. Radiol. 142 (9) (2021), 109833, https://doi.org/10.1016/j.ejrad.2021.109833.

[10] S.H. Choi, J.K. Han, J.M. Lee, K.H. Lee, S.H. Kim, J.Y. Lee, B.I. Choi, Differentiating malignant from benign common bile duct stricture with multiphasic helical CT, Radiology 236 (1) (2005) 178–183, https://doi.org/10.1148/radiol.2361040792.

[11] S.J. Park, J.K. Han, T.K. Kim, B.I. Choi, Three-dimensional spiral CT cholangiography with minimum intensity projection in patients with suspected obstructive biliary disease: comparison with percutaneous transhepatic cholangiography, Abdom. Imaging 26 (3) (2001) 281–286, https://doi.org/10.1007/s002610000140.

[12] E.P. Tamm, A. Balachandran, P. Bhosale, J. Szklaruk, Update on 3D and multiplanar MDCT in the assessment of biliary and pancreatic pathology, Abdom. Imaging 34 (1) (2009) 64–74, https://doi.org/10.1007/s00261-008-9416-4.

[13] M.M. Al-Hawary, I.R. Francis, S.T. Chari, E.K. Fishman, D.M. Hough, D.S. Lu, M. Macari, A.J. Megibow, F.H. Miller, K.J. Mortele, N.B. Merchant, R.M. Minter, E. P. Tamm, D.V. Sahani, D.M. Simeone, Pancreatic ductal adenocarcinoma radiology reporting template: consensus statement of the Society of Abdominal Radiology and the American Pancreatic Association, Gastroenterology 146 (1) (2014) 291–304, https://doi.org/10.1053/j.gastro.2013.11.004.

[14] M.A. Tempero, M.P. Malafa, M. Al-Hawary, H. Asbun, A. Bain, S.W. Behrman, A. B. Benson III, E. Binder, D.B. Cardin, C. Cha, E.G. Chiorean, V. Chung, B. Czito, M. Dillhoff, E. Dotan, C.R. Ferrone, J. Hardacre, W.G. Hawkins, J. Herman, A. H. Ko, S. Komanduri, A. Koong, N. LoConte, A.M. Lowy, C. Moravek, E. K. Nakakura, E.M. O'Reilly, J. Obando, S. Reddy, C. Scaife, S. Thayer, C.D. Weekes, R.A. Wolff, B.M. Wolpin, J. Burns, S. Darlow, Pancreatic adenocarcinoma, version 2.2017, NCCN Clinical Practice Guidelines in Oncology, JNCCN J. Natl. Compr. Cancer Netw. 15 (8) (2017) 1028–1061, https://doi.org/10.6004/jnccn.2017.0131.

[15] Y. Yamashita, Y. Komohara, M. Takahashi, M. Uchida, N. Hayabuchi, T. Shimizu, I. Narabayashi, Abdominal helical CT: evaluation of optimal doses of intravenous contrast material—a prospective randomized study, Radiology 216 (3) (2000) 718–723, https://doi.org/10.1148/radiology.216.3.r00se26718.

[16] S.M. Tao, J.L. Wichmann, U.J. Schoepf, S.R. Fuller, G.M. Lu, L.J. Zhang, Contrast-induced nephropathy in CT: incidence, risk factors and strategies for prevention, Eur. Radiol. 26 (9) (2016) 3310–3318, https://doi.org/10.1007/s00330-015-4155-8.

[17] D. Marin, D.T. Boll, A. Mileto, R.C. Nelson, State of the art: dual-energy CT of the abdomen, Radiology 271 (2) (2014) 327–342, https://doi.org/10.1148/radiol.14131480.

[18] M.J. Siegel, R.K. Kaza, D.N. Bolus, D.T. Boll, N.M. Rofsky, C.N. De Cecco, W. D. Foley, D.E. Morgan, U.J. Schoepf, D.V. Sahani, W.P. Shuman, T.J. Vrtiska, B. M. Yeh, L.L. Berland, White paper of the Society of Computed Body Tomography and Magnetic Resonance on dual-energy CT, part 1: technology and terminology, J. Comput. Assist. Tomogr. 40 (6) (2016) 841–845, https://doi.org/10.1097/RCT.0000000000000531.

[19] A. Padole, R.D. Ali Khawaja, M.K. Kalra, S. Singh, CT radiation dose and iterative reconstruction techniques, AJR Am. J. Roentgenol. 204 (4) (2015) W384–W392, https://doi.org/10.2214/AJR.14.13241.

[20] S.H. Kim, M.J. Kim, H.J. Lee, S.H. Cho, Comparison of full- and half-dose image reconstruction with filtered back projection or sinogram-affirmed iterative reconstruction in dual-source single-energy MDCT urography, AJR Am. J. Roentgenol. 211 (3) (2018) 641–648, https://doi.org/10.2214/AJR.17.19370.

[21] S. Choy, D. Parhar, K. Lian, H. Schmiedeskamp, L. Louis, T. O'Connell, P. McLaughlin, S. Nicolaou, Comparison of image noise and image quality between full-dose abdominal computed tomography scans reconstructed with weighted filtered back projection and half-dose scans reconstructed with improved sinogram-affirmed iterative reconstruction (SAFIRE*), Abdom. Radiol. 44 (1) (2019) 355–361, https://doi.org/10.1007/s00261-018-1687-9.

[22] N. Rassouli, H. Chalian, P. Rajiah, A. Dhanantwari, L. Landeras, Assessment of 70-keV virtual monoenergetic spectral images in abdominal CT imaging: a comparison study to conventional polychromatic 120-kVp images, Abdom. Radiol. 42 (10) (2017) 2579–2586, https://doi.org/10.1007/s00261-017-1151-2.

[23] P. Leyendecker, V. Faucher, A. Labani, V. Noblet, F. Lefebvre, P. Magotteaux, M. Ohana, C. Roy, Prospective evaluation of ultra-low-dose contrast-enhanced 100-kVabdominal computed tomography with tin filter: effect on radiation dose reduction and image quality with a third-generation dual-source CT system, Eur. Radiol. 29 (4) (2019) 2107–2116, https://doi.org/10.1007/s00330-018-5750-2.

[24] S.Y. Choi, J.H. Kim, H.J. Park, J.K. Han, Preoperative CT findings for prediction of resectability in patients with gallbladder cancer, Eur. Radiol. 29 (12) (2019) 6458–6468, https://doi.org/10.1007/s00330-019-06323-4.

[25] S. Kinner, V. Steinweg, S. Maderwald, A. Radtke, G. Sotiropoulos, M. Forsting, T. Schroeder, Bile duct evaluation of potential living liver donors with bile duct evaluation of potential living liver donors with Gd-EOB-DTPA enhanced MR cholangiography: single-dose, double dose or half-dose contrast enhanced imaging, Eur. J. Radiol. 83 (5) (2014) 763–767, https://doi.org/10.1016/j.ejrad.2014.02.012.

[26] X.P. Wu, J.M. Ni, Z.Y. Zhang, F.Q. Lu, B. Li, H.H. Jin, T. Dai, Preoperative evaluation of malignant perihilar biliary obstruction: negative-contrast CT cholangiopancreatography and CT angiography versus MRCP and MR angiography, AJR Am. J. Roentgenol. 205 (4) (2015) 780–788, https://doi.org/10.2214/AJR.14.13983.

[27] C. McCollough, T. Branham, V. Herlihy, M. Bhargavan, L. Robbins, K. Bush, M. McNitt-Gray, J.T. Payne, T. Ruckdeschel, D. Pfeiffer, D. Cody, R. Zeman, Diagnostic reference levels from the ACR CT accreditation program, J. Am. Coll. Radiol. 8 (11) (2011) 795–803, https://doi.org/10.1016/j.jacr.2011.03.014.

[28] Y. Ohno, D. Takenake, T. Kanda, T. Yoshikawa, S. Matsumoto, N. Sugihara, K. Sugimura, Adaptive iterative dose reduction using 3D processing for reduced- and low-dose pulmonary CT: comparison with standard-dose CT for image noise reduction and radiological findings, AJR Am. J. Roentgenol. 199 (4) (2012) W477–W485, https://doi.org/10.2214/AJR.11.8275.

[29] T. Yamashiro, T. Miyara, O. Honda, H. Kamiya, K. Murata, Y. Ohno, N. Tomiyama, H. Moriya, M. Koyama, S. Noma, A. Kamiya, Y. Tanaka, S. Murayama, Adaptive iterative dose reduction using three dimensional processing (AIDR 3D) improves chest CT image quality and reduces radiation exposure, PLOS ONE 9 (8) (2014), e105735, https://doi.org/10.1371/journal.pone.0105735.

[30] S.W. Kim, S.H. Kim, D.H. Lee, S.M. Lee, Y.S. Kim, J.Y. Jang, J.K. Han, Isolated main pancreatic duct dilatation: CT differentiation between benign and malignant causes, AJR Am. J. Roentgenol. 209 (5) (2017) 1046–1055, https://doi.org/10.2214/AJR.17.17963.

[31] E. Gibson, F. Giganti, Y. Hu, E. Bonmati, S. Bandula, K. Gurusamy, B. Davidson, S. P. Pereira, M.J. Clarkson, D.C. Barratt, Automatic multi-organ segmentation on abdominal CT with dense V-networks, IEEE Trans. Med. Imaging 37 (8) (2018) 1822–1834, https://doi.org/10.1109/TMI.2018.2806309.

[32] N. Tong, S.P. Gou, T.Y. Niu, S.Y. Yang, K. Sheng, Self-paced Dense Net with boundary constraint for automated multi-organ segmentation on abdominal CT

images, Phys. Med. Biol. 65 (13) (2020), 135011, https://doi.org/10.1088/1361-6560/ab9b57.
[33] J.R. Grajo, D.V. Sahani, Dual-energy CT of the abdomen and pelvis: radiation dose consideration, J. Am. Coll. Radiol. 15 (8) (2018) 1128–1132, https://doi.org/10.1016/j.jacr.2017.08.012.
[34] M. Akagi, Y. Nakamura, T. Higaki, K. Narita, Y. Honda, J. Zhou, Z. Yu, N. Akino, K. Awai, Deep learning reconstruction improves image quality of abdominal ultra-high-resolution CT, Eur. Radiol. 29 (11) (2019) 6163–6171, https://doi.org/10.1007/s00330-019-06170-3.